

Density Control by Second Harmonic X-Mode ECRH in LHD

Shin KUBO, Takashi SHIMOZUMA, Kenji TANAKA, Teruo SAITO¹⁾,
Yoshinori TATEMATSU¹⁾, Yasuo YOSHIMURA, Hiroe IGAMI, Takashi NOTAKE¹⁾,
Shigeru INAGAKI²⁾, Naoki TAMURA and LHD Experimental Group

National Institute for Fusion Science, Toki 509-5292, Japan

¹⁾*Research Center for Development of FIR Region, Fukui University, Fukui 910-8507, Japan*

²⁾*Research Institute of Applied Mechanics, Kyushu University, Kasuga 816-8580, Japan*

(Received 21 November 2007 / Accepted 27 March 2008)

Density clamping or pump-out phenomena is observed both in tokamaks and helical systems during additional heating, particularly high power density heating as electron cyclotron resonance heating (ECRH). Enhanced electron convective flux induced by a perpendicular acceleration of electrons is one of the candidates of the mechanism of these phenomena. The mechanism of the enhancement of the electron flux is investigated experimentally by comparing the density profile evolutions due to second harmonic X (X2) mode ECRH at the ripple top and bottom. The result suggests that ECRH-induced electron flux is one of the dominant mechanisms of density clamping, which can be used as a powerful tool for controlling the particles and the heat transport.

© 2008 The Japan Society of Plasma Science and Nuclear Fusion Research

Keywords: ECRH, density pump out, density control, direct loss, radial electric field

DOI: 10.1585/pfr.3.S1028

1. Introduction

Density clamping and pump-out are common phenomena in tokamaks and helical systems during high power density heating, particularly electron cyclotron resonance heating (ECRH). These phenomena are discussed in terms of the enhanced electron diffusion induced by the perpendicular acceleration in velocity space and the resultant electric field [1–3]. It is also suggested that a change in the electron temperature profile can enhance the radial particle diffusion due to a non-zero off-diagonal term in the transport matrix, which might be ascribed to the excitation of turbulent instabilities such as trapped electron modes [4]. The separation of the dominant mechanism of the density clamping is important for achieving effective ECRH from the view-point of both avoiding the confinement degradation and achieving better confinement.

If the change in the particle flux and the resultant electric field can be localized by local heating of ECRH, it can be a powerful knob for controlling the particle as well as the heat transport. In order to distinguish the effect of enhanced electron flux directly driven by ECRH or enhanced diffusion due to the change in the electron temperature or off-diagonal transport matrix, a series of experiments are performed. High power density local second harmonic X (X2) mode ECRH is applied to the NBI target plasma at the ripple top or bottom resonance for the different ripple conditions. The difference in the transient behavior of the density profile is observed between top and bottom heating or high- and low-ripple configurations. The X2 mode is selected because the perpendicular acceleration is more

enhanced in X2 than in the fundamental O (O1) mode. The role and mechanism of ECRH-induced particle flux in the particle and heat transport is discussed based on these phenomena. Such a degradation of the particle confinement is also observed in a tangential negative-ion neutral beam (N-NB) heated plasma in the Large Helical Device (LHD) for low-density discharges, where electron heating is dominant parallel to the magnetic field. Such observations also support the enhancement of the off-diagonal transport term. In order to distinguish both the effects, a series of experiments are performed. High power density second harmonic local ECRH is applied on the ripple top or bottom resonance position, where the width of the loss cone is wider for the bottom than for the top, but the expected power deposition profile is identical to each other in LHD. Experimental results comparing the ripple top and bottom heating cases are described in Section 2 with the detailed profile evolutions of the electron temperature and density. The analysis using these profile changes and possible applications is discussed in Section 3.

2. Experimental Results

2.1 Ripple top and bottom heating condition

For enhancing and clarifying the difference in the electron flux by ECRH, the heating positions and magnetic field strength are selected such that electrons on the ripple top and bottom at the same flux surfaces are heated on the vertically elongated cross section. The magnetic field strength and ECRH injection angles are adjusted to meet the second harmonic resonance condition (1.5 T for 84 GHz) at the desired position, as shown in Figs. 1 and 2.

author's e-mail: kubo@LHD.nifs.ac.jp

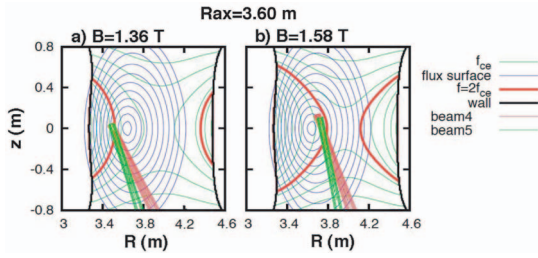


Fig. 1 Vertically elongated cross section of Mod- B , flux surfaces, second harmonic resonance layers and ECRH beams for ripple a) top and b) bottom heating geometries for $R_{ax} = 3.60$ m.

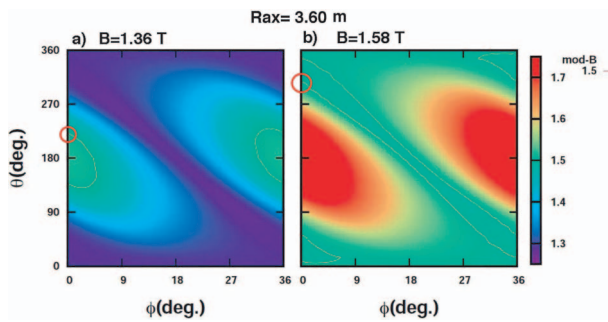


Fig. 2 Mod- B contour on toroidal poloidal plane on $\rho = 0.3$ of $R_{ax} = 3.60$ m configuration for ripple a) top and b) bottom heating geometries. Thin blue lines indicate the second harmonic resonance position for 84 GHz, and red circle indicates deposition region.

In Fig. 1 the vertically elongated cross section of the LHD with the Gaussian beams from the bottom for the magnetic field strength of a) 1.36 T and b) 1.58 T in the case of $R_{ax} = 3.60$ m configuration is shown. The second harmonic resonance layer is also shown in thick red lines. Strong interactions are expected near the cross section between the injected beam and the resonance. The power deposition profiles estimated from the multi-ray-tracing code [5] are confirmed to be identical and sharp at the normalized minor radius $\rho = 0.3$ for both cases. The half width of the deposition profile is 0.015 and 0.01 in ρ for the ripple top and bottom cases, respectively. Relative power deposition regions on the expanded $\rho = 0.3$ flux surface are indicated by the red circles in Fig. 2 for both magnetic field cases on a toroidal and poloidal angle plane. Here, the strength of the total magnetic field (Mod- B) is expressed in a color scale at $\rho = 0.3$ flux surface for a) the ripple top and b) the bottom heating conditions. Typical time evolutions of the plasma discharge are shown in Fig. 3. Ripple top and bottom second harmonic heating under the conditions shown in Figs. 1 and 2 superposed on the target NBI plasma. A set of discharges with the same initial density is selected. On the top column is shown the timing of the X2 ECRH pulse. The responses of an averaged electron density to the ripple top and bottom X2 ECRH

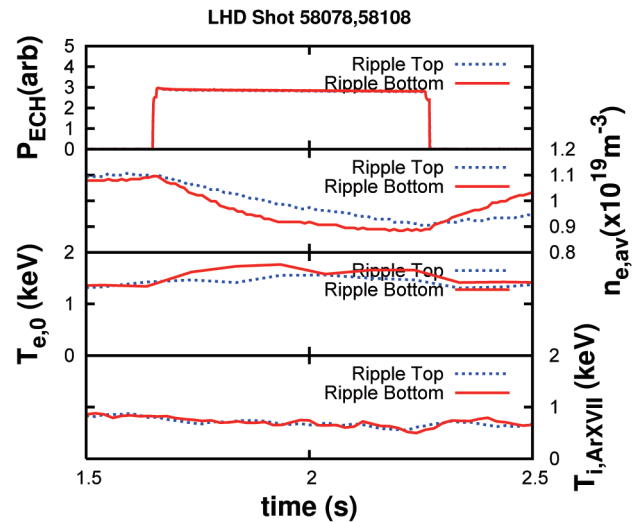


Fig. 3 Temporal evolutions of line averaged density, central electron and ion temperature for ripple top (dotted lines) and bottom (thick lines) ECRH on NB heated discharge.

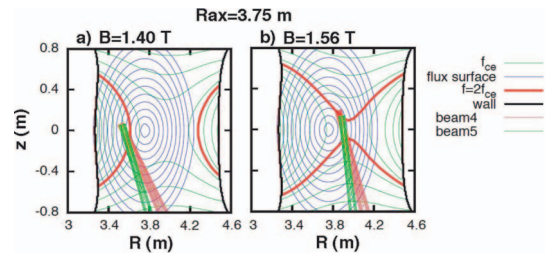


Fig. 4 Vertically elongated cross section of Mod- B , flux surfaces, second harmonic resonance layers and ECRH beams for ripple a) top and b) bottom heating geometries for $R_{ax} = 3.75$ m.

are plotted on the second column. The time response of the averaged electron density clearly differs in the case of ripple bottom heating case from that of the bottom case. For both cases, the electron temperature responds rapidly within 0.05 s, as indicated on the third column of Fig. 3. The ion temperature, as shown in the bottom column, does not show any responses to ECRH, and behaves identically for both cases.

In order to confirm the ECRH clamping effect due to the ripple top and bottom heating, similar experiments are performed for the smaller ripple condition. Here, the configuration $R_{ax} = 3.75$ m is chosen as a reference. In Figs. 4 and 5 are shown the injection conditions and mod- B structure in relation to the heating region. As is seen in Figs. 2 and 5, the ripple ratios defined by the ratio of the difference in the maximum and minimum magnetic field strength to the averaged one on $\rho = 0.3$ flux surface for the case of $R_{ax} = 3.60$ and 3.75 m are 0.15 and 0.1, respectively. Typical discharge waveforms are shown in Fig. 6 for the ripple top and bottom cases. The increases in the electron temperature and stored energy in both cases are clear, but the clamping effect is weak for both cases. The difference of the clamping effect for both cases needs to be analyzed in

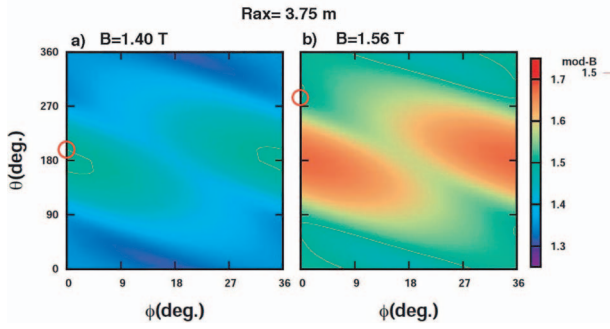


Fig. 5 Mod- B contour on toroidal poloidal plane on $\rho = 0.3$ of $R_{ax} = 3.75$ m configuration for ripple a) top and b) bottom heating geometries. Red line indicates the resonance position.

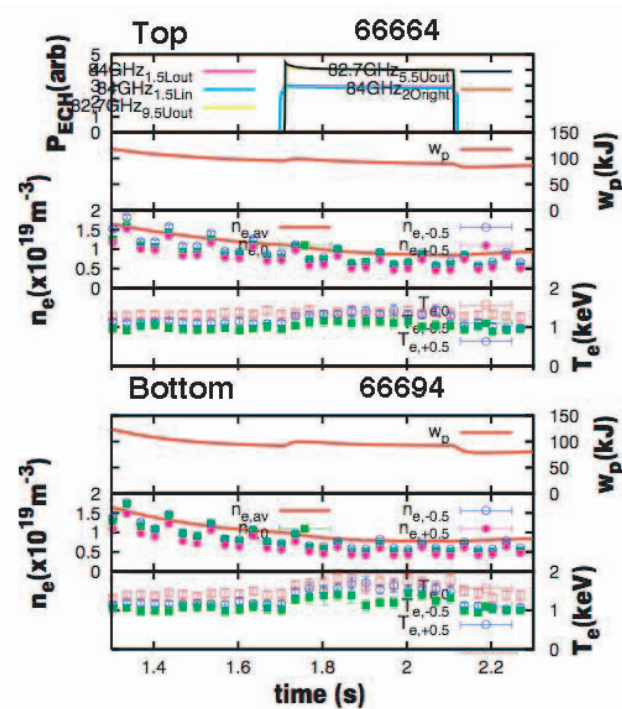


Fig. 6 Density profile at several time slices after ECH injection [a) and c)]. Time evolutions of the density at several spatial points b), and d) for ripple top [a) and b)] and bottom [c) and d)] heating cases.

detail, but it is clear from the comparison with $R_{ax} = 3.60$ m configuration that the density clamping is strongly related to the magnetic ripple rate at the heating region, implying that the ECRH-related physics plays an important role in the clamping phenomena.

2.2 Detailed comparison of electron temperature and density profile for $R_{ax} = 3.60$ m configuration

The time evolutions of the density, central electron, and ion temperature in response to ECRH on NB heated plasma for the ripple top and bottom resonance heating conditions are shown in Fig. 3. In both cases, density

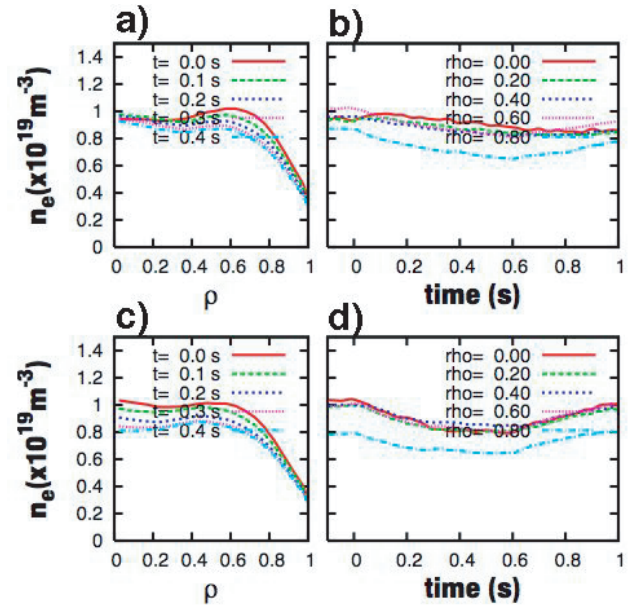


Fig. 7 Temperature profile at several time slices after ECH injection [a) and c)]. Time evolutions of the density at several spatial points b), and d) for ripple top [a) and b)] and bottom [c) and d)] heating cases.

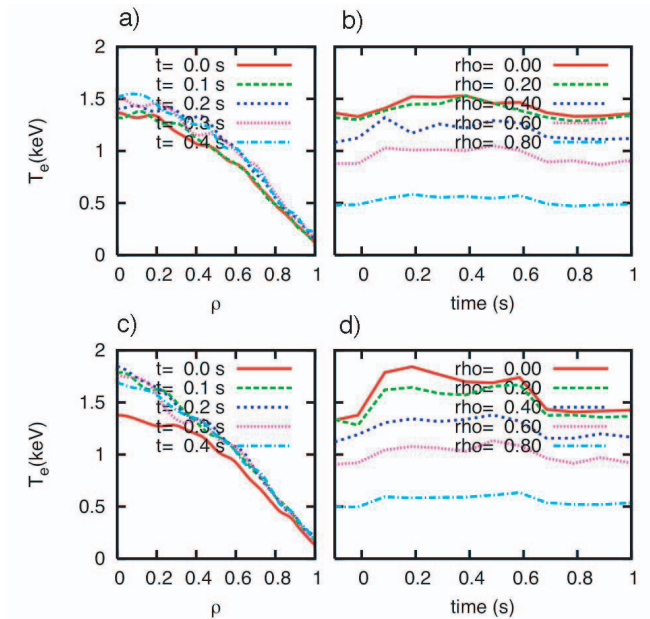


Fig. 8 Temporal evolutions of line averaged density, central electron and ion temperature for a) ripple top and b) bottom ECRH on NB heated discharge.

decrease is observed on ECRH, but the time behavior of the decrease in the density clearly changes according to the heating position. The line averaged density decreases faster in the ripple bottom heating case than in the top one. The decrease rate saturates in the time constant of 200 ms for the bottom heating case, whereas that for the top heating case remains constant during the ECRH injection of 500 ms. The electron temperature increases within 100 ms,

and remains almost constant during the injection for both cases. The profile changes of the density reconstructed using a multi-chord FIR interferometer are shown in Fig. 7. It should be noted that the density drops at $\rho \gtrsim 0.4$ but the central part is not affected by the ECRH injection for the top heating case, whereas it drops in almost the entire region for the bottom heating case. The change in the electron temperature profile at several timings during the ECRH phase and the temporal evolutions at several radial positions are shown in Fig. 8. The temperature increase of the central region for the case of ripple bottom due to ECRH is larger than with the ripple top case. In both cases, the profile change occurs within 100 ms, and remains almost constant after 100 ms from the ECRH injection. This means that the change in the density profile evolutions after 100 ms of the ECRH injection is attributed to the diagonal term and direct flux due to ECRH in the electron diffusion.

3. Discussion

Neglecting the source and sink term other than that due to ECRH, the diffusion equation is expressed in terms of the electron density $n_e(r, t)$ and temperature profiles $T_e(r, t)$ as

$$\Gamma_e(r, t) = D_{e,n}(r, t) \frac{\partial n_e(r, t)}{\partial r} + D_{e,T}(r, t) \frac{\partial T_e(r, t)}{\partial r} + \Gamma_{\text{ECH}}(r, t). \quad (1)$$

Here, $D_{e,n}(r, t)$ denotes the normal electron diffusion coefficient, and $D_{e,T}(r, t)$ is an off-diagonal element due to the electron temperature gradient. Then, the diffusion equation is expressed with this electron flux $\Gamma_e(r, t)$ as

$$\frac{\partial n_e(r, t)}{\partial t} = -\frac{\partial}{\partial r} \left(r \Gamma_e(r, t) \right). \quad (2)$$

Integrating over radius of Eq. (2) gives

$$\Gamma_e(r, t) = -\frac{1}{r} \int_0^r r' \frac{\partial n_e(r', t)}{\partial t} dr'. \quad (3)$$

Thus, total electron flux can be deduced from Eq. (3) by the experimentally observed quantity $n_e(r', t)$. In Fig. 9 are shown the change in the particle flux deduced from Eq. (3) for the ripple a) top and b) bottom cases. Fast increase of the flux at $\rho \gtrsim 0.3$ is clearer in the ripple bottom heating case than in the top case. The density gradient profile changes are also shown in Fig. 9 c) and d) for comparison. As is expected from Eq. (1), the correlations between a) and c) or b) and d) indicate the effect of normal diffusion coefficient, but there seems no clear correlation between them. Second term in Eq. (1) describes the off-diagonal term from the temperature gradient. As is described above, the temperature profile change occurs only at the beginning 100 ms after ECRH injection for both cases. So the correlation between the deduced flux and the temperature gradient should also be weak. These results indicate that the change in the deduced particle flux for the ripple top

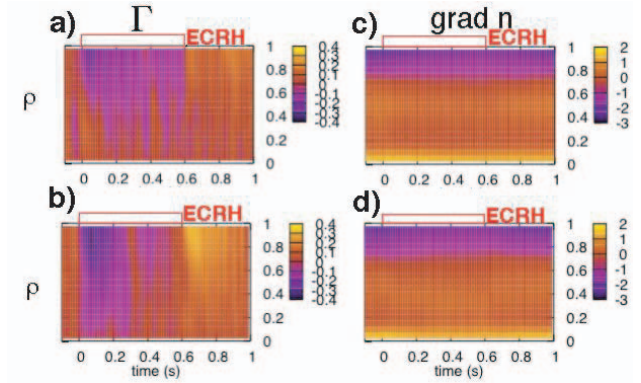


Fig. 9 Particle flux deduced from Eq. (3) for ripple a) top and b) bottom cases. c) and d) show a temporal change in the density gradient for each case.

and bottom cases are directly driven by ECRH, although the dynamical dependence of the diffusion coefficient on the temperature and its gradient, off-diagonal term and the effect of the radial electric field should be considered more carefully.

It is clear from above discussions that second harmonic X-mode ECRH works as an active electron flux driver. These results indicate the possibility to use ECRH for controlling the electron density profile, or as the driver of electron particle flux as well as heating source.

4. Conclusion

By applying ripple top and bottom second harmonic ECRH, the density clamping phenomena are investigated. From the comparison of the density clamping between different ripple cases ($R_{ax} = 3.60$ and 3.75 m), ECRH physics, i.e., perpendicular acceleration of the electron, is shown to play an important role in the clamping phenomena. This suggests that the ECRH can be used as a tool for controlling the local density. The direct electron flux by ECRH due to the enhanced ripple loss is one of the possible mechanisms of the difference in the temporal behaviors of the electron density profile. The effect of the formation of the radial electric field may have mitigated the degradation. Experimental and theoretical investigations of the effect of the radial electric field are left for future work.

Acknowledgement

The authors would like to thank the technical staff of ECRH and LHD for the continuous efforts to perform the experiments. This study is mainly performed under budget code NIFS05ULRR501-3.

- [1] K. Itoh *et al.*, J. Phys. Soc. Japan **58**, 482 (1989).
- [2] H. Sanuki *et al.*, Phys. Fluids **B2**, 2155 (1990).
- [3] H. Idei *et al.*, Fusion Eng. Des. **26**, 167 (1995).
- [4] C. Angioni *et al.*, Nuclear Fusion **44**, 167 (2004).
- [5] S. Kubo *et al.*, J. Plasma Fusion Res. SERIES **5**, 584 (2002).